

# The Scope of the $4\tau$ Channel in Higgs-strahlung and Vector Boson Fusion for the NMSSM No-Lose Theorem at the LHC

Alexander Belyaev<sup>1,2</sup>, Stefan Hesselbach<sup>3</sup>, Sami Lehti<sup>4</sup>, Stefano Moretti<sup>1</sup>,  
Alexander Nikitenko<sup>5,\*</sup>, Claire H. Shepherd-Themistocleous<sup>2</sup>

<sup>1</sup>*School of Physics & Astronomy, University of Southampton, Highfield, Southampton  
SO17 1BJ, UK*

<sup>2</sup>*Particle Physics Department, Rutherford Appleton Laboratory, Chilton, Didcot, Oxon  
OX11 0QX, UK*

<sup>3</sup>*IPPP, University of Durham, South Road, Durham DH1 3LE, UK*

<sup>4</sup>*Helsinki Institute of Physics, P.O. Box 64, 00014 Helsinki, Finland*

<sup>5</sup>*Blackett Laboratory, Physics Department, Imperial College, London SW7 2AZ, UK*

## Abstract

We study the potential of the  $h_1 \rightarrow a_1 a_1 \rightarrow 4\tau$  signal from the lightest scalar ( $h_1$ ) and pseudoscalar ( $a_1$ ) Higgs bosons to cover the parameter space of the Next-to-Minimal Supersymmetric Standard Model (NMSSM) at the Large Hadron Collider (LHC). We exploit a  $2\mu + 2\text{jets}$  signature from four  $\tau$ 's decays (accompanied by missing transverse energy), resorting to both Higgs-strahlung (HS), by triggering on leptonic  $W^\pm$  decays, and Vector Boson Fusion (VBF), by triggering on two same sign non-isolated muons.

---

\* On leave from ITEP, Moscow, Russia.

# 1 Introduction

The NMSSM [1–13], which contains a singlet/singlino superfield in addition to the particle content of the Minimal Supersymmetric Standard Model (MSSM), has various advantages with respect to the MSSM such as the solution of the  $\mu$  problem and the smaller fine-tuning<sup>1</sup> [18–20]. The additional singlet field results in one new CP-even and one new CP-odd state in the Higgs sector which consists of three CP-even mass eigenstates ( $h_{1,2,3}$ ) and two CP-odd states ( $a_{1,2}$ ) in the NMSSM. In contrast to the MSSM, it is not certain that even at least one Higgs boson can be found at the CERN Large Hadron Collider (LHC) within the NMSSM. This problem can be created by the additional singlet states in the Higgs sector leading to invisible decay channels of the SM-like Higgs states. Of particular relevance for the Higgs search at the LHC in the NMSSM are the decays of the lightest CP-even Higgs into lighter CP-odd states,  $h_1 \rightarrow a_1 a_1$ . This channel has been claimed to be the only means to establish a no-lose theorem for the NMSSM [21–31], at least in parameter regions where the Supersymmetric (SUSY) partners of ordinary Standard Model (SM) objects are made suitable heavy. Also notice that the  $h_1$  state could well be below the LEP limit on the SM Higgs mass, of 114 GeV, albeit with weakened couplings to ordinary matter.

In this letter we will focus on NMSSM parameter regions with light  $a_1$  states (light  $a_1$  scenario) with  $M_{a_1} < 2m_b$  where the decay  $a_1 \rightarrow b\bar{b}$  is not possible. In these parameter regions with large  $\text{BR}(a_1 \rightarrow \tau^+\tau^-)$  the scope of  $h_1 \rightarrow a_1 a_1$  decays into  $jj\tau^+\tau^-$  pairs (where  $j$  represents a jet of either heavy or light flavour and where the  $\tau$ 's decay leptonically) has been found to be rather questionable [32]. Hence, here we investigate the scope of the  $4\tau$  channel, wherein two  $\tau$ 's are searched for in their muonic decays, while the other two are selected via their hadronic ones. In doing so, we exploit both the HS and VBF production channels.

The plan of the paper is as follows. In section 2 the results of a detailed parameter scan are discussed identifying the parameter regions with light  $a_1$  and possibly light  $h_1$  with  $M_{h_1} < 114$  GeV. In section 3 the  $h_1$  production and decay processes are simulated with the PYTHIA event generator [33] and the prospects for the determination of the NMSSM Higgs bosons in the channel  $h_1 \rightarrow a_1 a_1 \rightarrow 4\tau$  are discussed. We then conclude in section 4.

## 2 The low-energy NMSSM parameter space for the light $a_1$ scenario

Here we investigate the NMSSM parameter space for  $M_{a_1} < 2m_b$ , with particular interest in the cases where the aforementioned  $h_1 \rightarrow a_1 a_1 \rightarrow 4\tau$  decays may be visible at the LHC from HS and/or VBF production processes. The NMSSM Higgs at the Electro-Weak (EW) scale is uniquely defined by fourteen parameters: the ratio of the doublet Higgs

---

<sup>1</sup>Alternative formulations of the MSSM with an additional singlet/singlino superfield — known as the Minimal Non-minimal Supersymmetric Standard Model (MNSSM) and new Minimally-extended Supersymmetric Standard Model or nearly-Minimal Supersymmetric Standard Model (nMSSM) — also exist [14–17].

vacuum expectation values (VEVs)  $\tan\beta$ , the trilinear couplings in the superpotential  $\lambda$  and  $\kappa$ , the corresponding soft SUSY breaking parameters  $A_\lambda$  and  $A_\kappa$ , the effective  $\mu$  parameter  $\mu = \lambda\langle S \rangle$  (where  $\langle S \rangle$  denotes the VEV of the singlet Higgs field), the gaugino mass parameters  $M_1$ ,  $M_2$  and  $M_3$ , the squark and slepton trilinear couplings  $A_t$ ,  $A_b$  and  $A_\tau$ , and the squark and slepton mass parameters  $M_{f_L}$  and  $M_{f_R}$ . In the following we will establish the NMSSM parameter regions, defined in terms of the above inputs, that survive present theoretical and experimental constraints.

## 2.1 Full NMSSM parameter scan

First we perform a ‘wide’ scan over the full NMSSM parameter space, where the numerical values over which the parameters have been varied are:

$$\begin{aligned} -1000 \text{ GeV} < A_\kappa < 100 \text{ GeV}, \quad -5 \text{ TeV} < A_\lambda < 5 \text{ TeV}, \quad 100 \text{ GeV} < \mu < 1000 \text{ GeV}, \\ 10^{-5} < \lambda, \kappa < 0.7, \quad 1.5 < \tan\beta < 50 \end{aligned} \quad (1)$$

while the remaining parameters (entering the Higgs sector at loop-level) were fixed at

$$M_1/M_2/M_3 = 150/300/1000 \text{ GeV}, \quad A_t = A_b = A_\tau = 2.5 \text{ TeV}, \quad M_{f_L} = M_{f_R} = 1 \text{ TeV}, \quad (2)$$

resulting in a heavy spectrum of the SUSY partners of  $\mathcal{O} = 1 \text{ TeV}$  (except for the U(1) and SU(2) gauginos). This scan (as well as all the others in the remainder of this letter) has been performed by using the NMSSMTools package [34–36], which calculates NMSSM spectra (masses, couplings and decay rates) and takes into account experimental inputs including LEP limits,  $B$ -physics bounds as well as constraints on the relic density of cold dark matter (DM) stemming from the results obtained by the Wilkinson Microwave Anisotropy Probe (WMAP) [37].

In Fig. 1 we present the results of this scan in form of scatter plots, corresponding to  $10^7$  generated points, where about  $2.7 \times 10^5$  points survive all constraints but the DM constraints (red points) and about  $7.6 \times 10^4$  points survive all constraints (black and green points). The bands between  $115 \text{ GeV} \lesssim M_{h_1} \lesssim 130 \text{ GeV}$  appear because in a majority of the generated points the  $h_1$  has SM-like properties where the lower bound of the band is given by the LEP Higgs limit and the upper bound by the theoretical upper limit of the  $h_1$  mass in the NMSSM. For the points with  $M_{h_1} \lesssim 115 \text{ GeV}$  the  $h_1$  couplings to SM gauge bosons are suppressed, hence the LEP Higgs limit is not applicable. Though only 17 points with  $M_{a_1} < 10 \text{ GeV}$  survive (green points), one can see from Fig. 1(a) that small  $|A_\kappa|$ ’s are preferred while Fig. 1(b) indicates the preference for large positive  $A_\lambda$ .

## 2.2 Scan for narrowed $A_\kappa$ range

The results of Fig. 1 (especially the preference for small  $A_\kappa$ ’s) motivated us to ‘narrow’ the range of the parameters, by scanning it over the intervals

$$-20 \text{ GeV} < A_\kappa < 25 \text{ GeV}, \quad -2 \text{ TeV} < A_\lambda < 4 \text{ TeV}, \quad 100 \text{ GeV} < \mu < 300 \text{ GeV}, \quad (3)$$

and the rest of the parameters as in Eq. (1). Fig. 2, based on  $10^7$  generated points resulting in  $2.9 \times 10^5$  points surviving all but the DM constraints (red points) and  $4.0 \times 10^5$  points

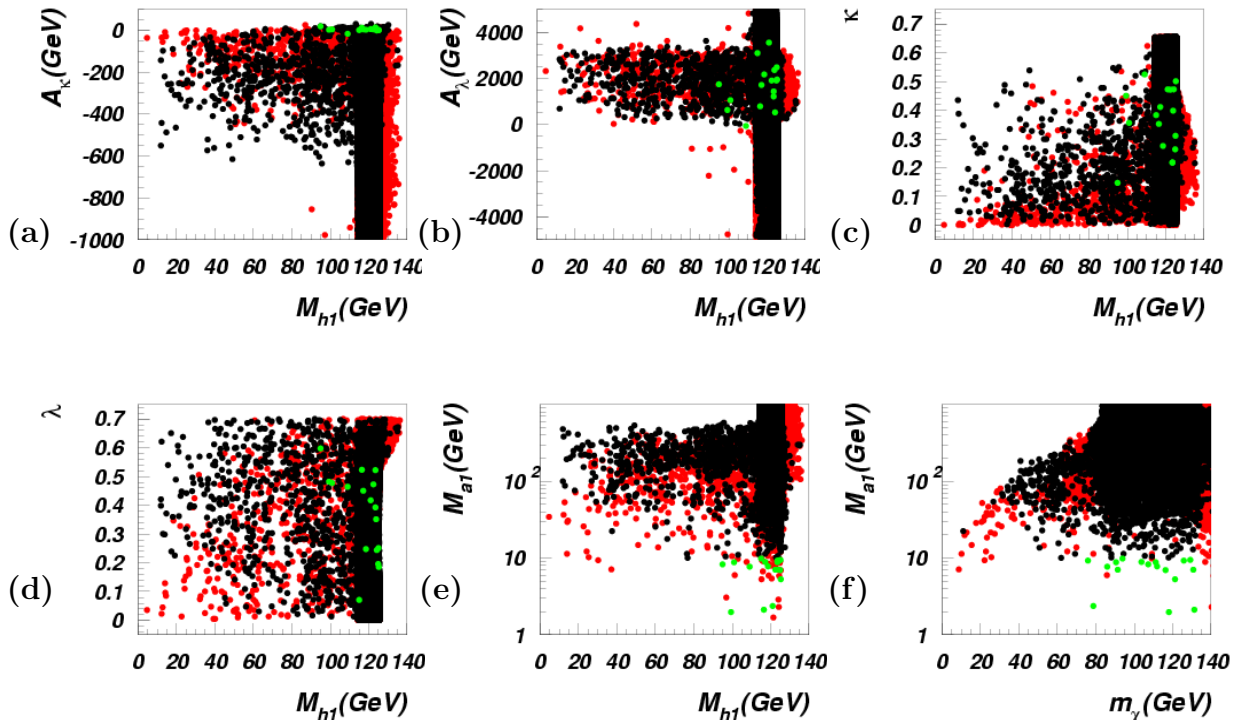


Figure 1: Results of the ‘wide’ scan over the full NMSSM parameter space, Eq. (1), mapped onto the planes: (a)  $[A_\kappa, M_{h_1}]$ , (b)  $[A_\lambda, M_{h_1}]$ , (c)  $[\kappa, M_{h_1}]$ , (d)  $[\lambda, M_{h_1}]$ , (e)  $[M_{a_1}, M_{h_1}]$ , (f)  $[M_{a_1}, m_{\chi_1^0}]$ . Colour code: red – all constraints are satisfied but relic density (above WMAP constraint:  $\Omega h^2 > 0.11$ ); black – all constraints are satisfied,  $M_{a_1} > 10$  GeV; green – all constraints are satisfied,  $M_{a_1} < 10$  GeV.

surviving all constraints (black and green points), shows that this is precisely the region where a large portion of the NMSSM parameter points with  $M_{a_1} < 10$  GeV (here  $3.3 \times 10^3$  green points) are found. Now we can also see certain correlations and other interesting features onsetting in the  $M_{a_1} < 10$  GeV region:

1. values of  $A_\lambda > 0$  are preferred, see Fig. 2(b);
2. for points with low  $M_{h_1}$  small values of  $|A_\kappa|$  (Fig. 2(a)) as well as small values of  $\kappa$  (Fig. 2(c)) are preferred;
3. in the  $M_{a_1} < 10$  GeV region of our interest,  $M_{h_1}$  as low as 20 GeV can appear (Fig. 2(e)).

### 2.3 Final scan for the light $a_1$ scenario

We have then performed a ‘final’ scan over the NMSSM parameter space by requiring  $M_{a_1} < 10$  GeV additionally to Eq. (3). At this stage, we recast the NMSSM parameter space in terms of the quantities entering  $h_1$  HS and VBF production and  $h_1 \rightarrow a_1 a_1 \rightarrow 4\tau$

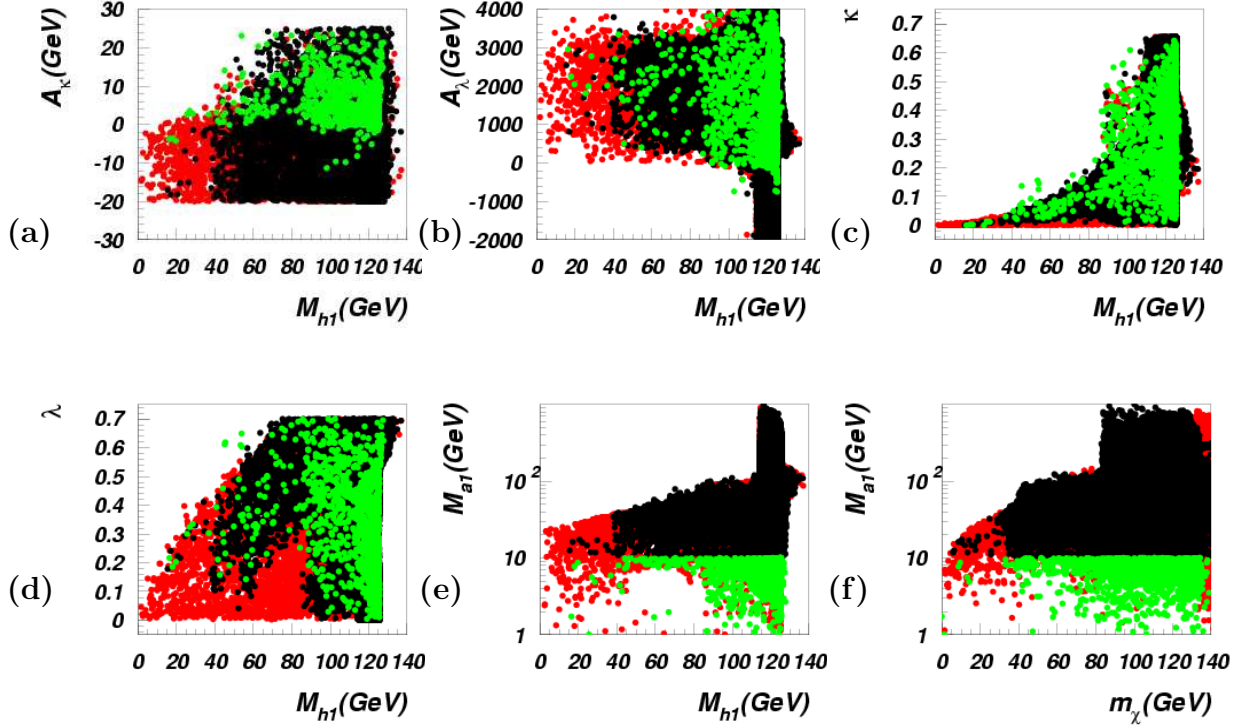


Figure 2: Results of the scan over the ‘narrowed’ NMSSM parameter space, i.e., analogous to Fig. 1 but for  $-20 \text{ GeV} < A_{\kappa} < 25 \text{ GeV}$ ,  $-2 \text{ TeV} < A_{\lambda} < 4 \text{ TeV}$ ,  $100 \text{ GeV} < \mu < 300 \text{ GeV}$ . The individual plots and the colour code are the same as in Fig. 1.

decays. The results of this scan ( $10^8$  generated points, resulting in  $3.9 \times 10^4$  points with  $M_{a_1} < 10 \text{ GeV}$  surviving all constraints) are shown in Fig. 3, where the colours were chosen to indicate the measure of decoupling of the lightest CP-even Higgs boson,  $h_1$ , from the SM limit (denoted simply by  $H$ ). This measure of decoupling was defined through the ratio of the coupling strength (squared) of the  $ZZh_1$  vertex in the NMSSM relative to the SM case (in fact, this is the same for couplings to  $W^{\pm}$  gauge bosons):  $R_{ZZh} = (g_{ZZh_1}^{\text{NMSSM}}/g_{ZZH}^{\text{SM}})^2$ . One should notice that both HS,  $pp \rightarrow Vh_1$ , and VBF,  $pp \rightarrow jjV^*V^* \rightarrow jjh_1$ , rates ( $V = Z, W^{\pm}$ ) are directly proportional to  $R_{ZZh}$  and are suppressed in the non-decoupling regime whenever  $R_{ZZh}$  is essentially smaller than unity.

From Figs. 3 and 4 one can see the following important features of the  $M_{a_1} < 2m_b \approx 10 \text{ GeV}$  scenario:

1. The lighter the Higgs  $h_1$  the more significant should be the NMSSM deviations from the SM case, e.g., for any  $M_{h_1} < 50 \text{ GeV}$  any  $R_{ZZh}$  is limited to be  $< 0.5$ , as dictated by LEP constraints [38, 39] (this correlation is illustrated in a more clear way in Fig. 4(a), presenting the  $R_{ZZh}$  versus  $M_{h_1}$  plane, which exhibits the typical pattern of the LEP Higgs exclusion curve [39]).
2. In the  $M_{h_1} < 40 \text{ GeV}$  region  $A_{\lambda}$  is always positive (Fig. 3(b)),  $\lambda < 0.45$  (Fig. 3(d)) while  $\kappa < 0.1$  (Figs. 3(c), 4(b)), which corresponds to an approximate Peccei-Quinn

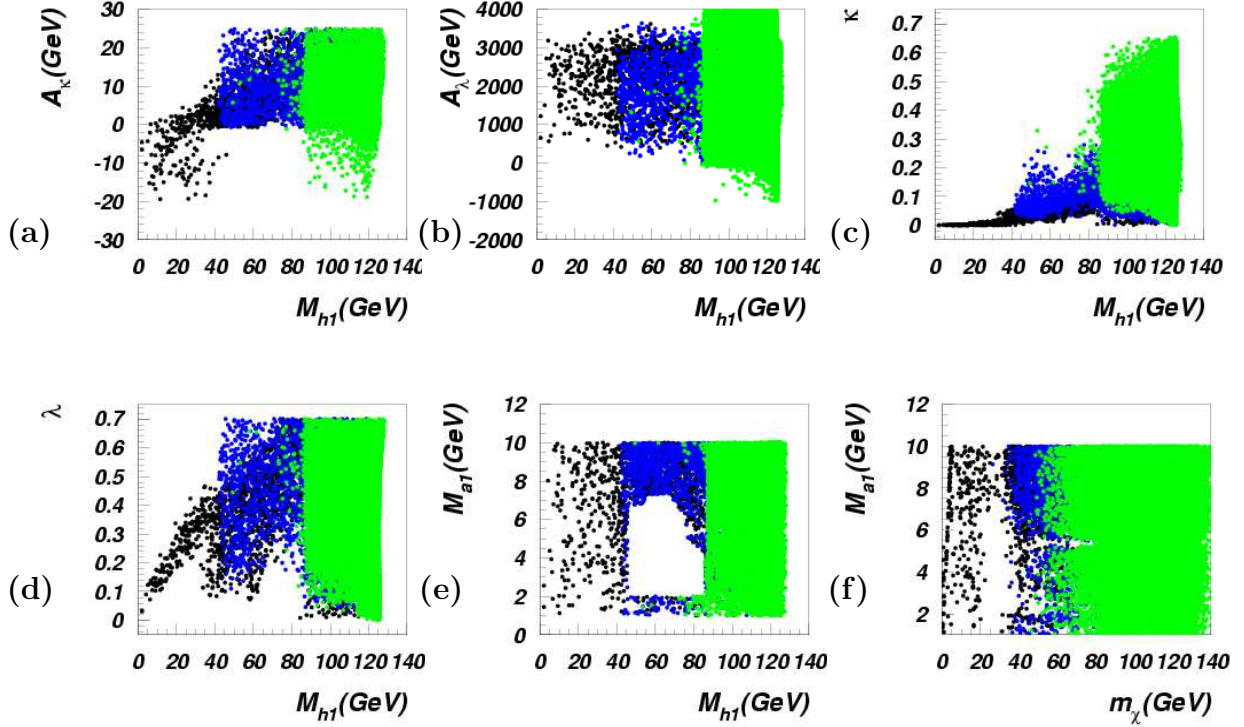


Figure 3: Results of the ‘final’ NMSSM parameter scan, i.e., with  $M_{a_1} < 10$  GeV and with Eq. (3) enforced. The black, blue and green colours indicate the cases  $R_{ZZh} < 0.1$ ,  $0.1 < R_{ZZh} < 0.5$  and  $R_{ZZh} > 0.5$ , respectively (where  $R_{ZZh}$  is defined in the text). The individual plots are the same as in Fig. 1.

(PQ) symmetry ( $\kappa \rightarrow 0$  and  $\kappa A_\kappa \rightarrow 0$ ) [13, 40]. However, for  $M_{h_1} \gtrsim M_Z$  the whole range  $0 < \kappa < \kappa_{\max} \sim 0.7$  is populated. Hence an approximate PQ symmetry is not necessary for the  $M_{a_1} < 2m_b \approx 10$  GeV and  $M_{h_1} \gtrsim M_Z$  scenario while some fine-tuning ensuring  $|A_\kappa| \ll |A_\lambda|$  is present.

- One should further notice the correlation between the singlet nature of the  $h_1$  and the singlino component of the lightest neutralino as well as the correlation between their masses, which are visualised in Fig. 4(c) and (d), respectively. These correlations take place to satisfy WMAP constraints on relic density. In fact, in the lower-left corner Fig. 4(d) we can clearly observe  $\chi_1^0 \chi_1^0 \rightarrow h_1$  the annihilation corridor for  $M_{h_1} < 80$  GeV, along which  $2m_{\chi_1^0} \simeq M_{h_1}$  that allows one to lower down the neutralino relic density to a level consistent with experimental constraints. In this corridor  $\chi_1^0$  and  $h_1$  have significant singlino and singlet components, respectively. At the very bottom of Fig. 4(d) we can further see another DM motivated region with very light ( $< 5$  GeV) neutralino where  $2m_{\chi_1^0} \simeq M_{a_1}$  provides the  $\chi_1^0 \chi_1^0 \rightarrow a_1$  annihilation corridor. This region is also represented in Fig. 3(f) as a border-line at the left edge of the parameter space. These two representative DM motivated regions appear because the NMSSM structure requires  $h_1$  to be a singlet and  $\chi_1^0$  to be a singlino for  $M_{a_1} < 10$  GeV and low  $M_{h_1}$ .

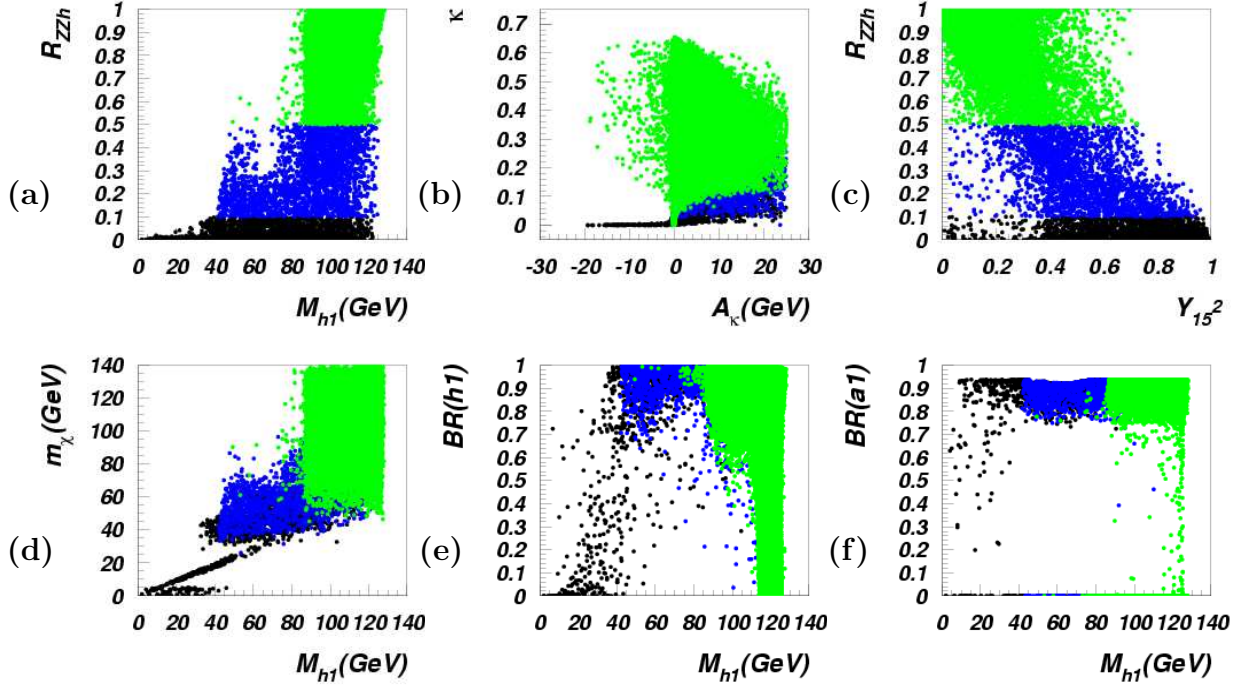


Figure 4: Results of the ‘final’ NMSSM parameter scan, i.e., with  $M_{a_1} < 10$  GeV and with Eq. (3) enforced: (a)  $R_{ZZh}$  (see text) versus  $M_{h_1}$ , (b)  $\kappa$  versus  $A_\kappa$ , (c)  $R_{ZZh}$  versus the singlino component  $y_{15}^2$  of the lightest neutralino  $\chi_1^0$ , (d)  $m_{\chi_1^0}$  versus  $M_{h_1}$ , (e)  $\text{BR}(h_1 \rightarrow a_1 a_1)$  versus  $M_{h_1}$ , (f)  $\text{BR}(a_1 \rightarrow \tau^+ \tau^-)$  versus  $M_{h_1}$ . The colour coding is the same as in Fig. 3.

4. The branching ratios  $\text{BR}(h_1 \rightarrow a_1 a_1)$  (Fig. 4(e)) and  $\text{BR}(a_1 \rightarrow \tau^+ \tau^-)$  (Fig. 4(f)) are large for a large fraction of the parameter points with  $M_{a_1} < 2m_b \approx 10$  GeV which is crucial for the  $h_1 \rightarrow a_1 a_1 \rightarrow 4\tau$  mode analysed in the next section.

### 3 Phenomenology of the light $a_1$ scenario

As a final step of our analysis, we have combined the production rates of VBF and HS with selection efficiencies evaluated by generating these processes within the PYTHIA Monte Carlo (MC) generator. The latter have been estimated in presence of experimental-like cuts, after parton showering and hadronisation and with underlying events turned on. The jets, in particular in the VBF analysis, were found with the PYTHIA routine PYCELL using the approximate CMS calorimeter tower granularity and cone size 0.5. No detector smearing of the jet energy is applied, however, we do not expect a significant reduction of the event selection efficiency once this is enforced<sup>2</sup>.

The  $h_1 \rightarrow a_1 a_1 \rightarrow \tau^+ \tau^- \tau^+ \tau^-$  mode from VBF  $h_1$  production has been considered for

<sup>2</sup>The selection efficiency is related to a cut on jet transverse energy  $E_T$  and since we cut right on the peak of the tagging jet  $E_T$  distribution we do not expect jet energy smearing to affect this efficiency substantially.

the  $\mu^\pm\mu^\pm\tau_{\text{jet}}^\mp\tau_{\text{jet}}^\mp$  final state containing two same sign muons and two same sign  $\tau$  jets ( $\tau$  jet means the  $\tau$  lepton decaying hadronically,  $\tau \rightarrow \text{hadrons} + \nu$ ). The  $\tau$  leptons from the light  $a_1$  decay are approximately collinear. Fig. 5(a) shows the separation in the  $(\eta, \phi)$  space between the two  $\tau$  leptons and between the muon and the  $\tau$  jet in the decay chain  $a_1 \rightarrow \tau\tau \rightarrow \mu\nu\nu + \tau_{\text{jet}}\nu$  for the benchmark point P2,  $M_{h_1} = 120.2$  GeV and  $M_{a_1} = 9.1$  GeV, proposed in [18, 20]. The non-isolated, di-muon High Level (HL) trigger is needed

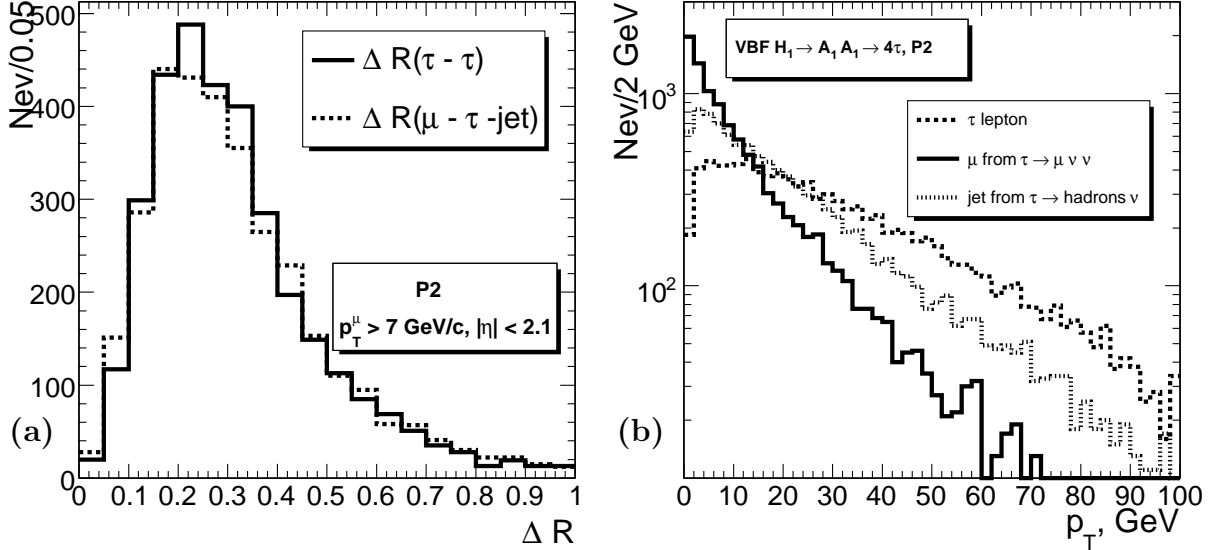


Figure 5: (a) Separation in  $(\eta, \phi)$  space between the two  $\tau$  leptons and between the muon and the  $\tau$  jet from the  $a_1 \rightarrow \tau\tau \rightarrow \mu\nu\nu + \tau_{\text{jet}}\nu$  decay chain in the VBF  $h_1 \rightarrow a_1 a_1 \rightarrow \tau^+ \tau^- \tau^+ \tau^- \rightarrow \mu^\pm \mu^\pm \tau_{\text{jet}}^\mp \tau_{\text{jet}}^\mp$  channel for the benchmark point P2:  $M_{h_1} = 120.2$  GeV,  $M_{a_1} = 9.1$  GeV. (b) Distributions of  $p_T^\tau$ ,  $p_T^\mu$  and  $p_T^{\tau \text{ jet}}$  for the point P2.

to select the signal events. The standard CMS di-muon trigger with relaxed isolation has a di-muon threshold 10 GeV on both muons for  $\mathcal{L} = 2 \times 10^{33} \text{ cm}^{-2} \text{ s}^{-1}$  [41]. The muons from the signal events are very soft as one can see in Fig. 5(b), thus lower thresholds are needed. For example with the 7 GeV threshold the efficiency is increased approximately by a factor of two. However the QCD background rate is also increased by approximately a factor of two [42] which is not acceptable. In order to cope with the rate, the same sign relaxed di-muon trigger was introduced recently in the CMS trigger table [43]. The rate of di-muons from  $b\bar{b}$  production is reduced by a factor of four when asking for two muons of the same sign at the threshold 5 GeV. The off-line selection strategy requires the presence of the two same sign, non-isolated muons with one track within a cone 0.6 around each muon direction, thus selecting the one prong  $\tau$  decays. The full list of off-line selections is:

- two same sign muons with  $p_T > 7$  GeV and  $|\eta| < 2.1$  with one track of  $p_T > 2$  GeV in a cone 0.6 around each muon. The muon and the track should have opposite charge;
- two  $\tau$  jets with  $p_T > 10$  GeV,  $|\eta| < 2.1$ ;



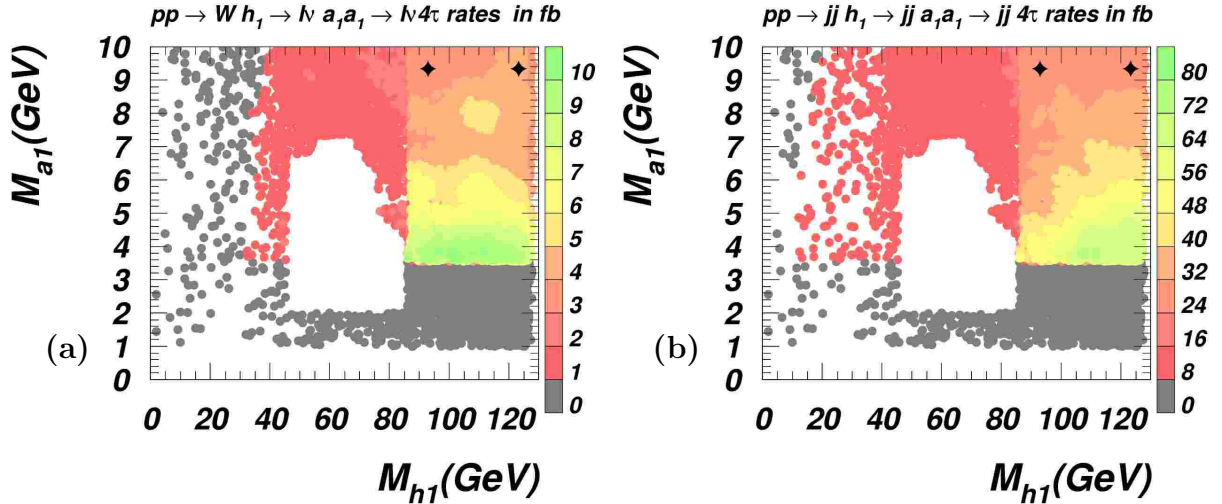


Figure 6: Cross sections (including all relevant branching ratios) for HS (a) and VBF (b) after the selection cuts described in the text. The population of points used correspond to that of the ‘final scan’ described previously. Black diamonds correspond to the benchmark P2 (right) and P3 (left) from Refs. [18, 20].

- two jets with  $p_T > 30$  GeV,  $|\eta| < 4.5$ .

The  $h_1 \rightarrow a_1 a_1 \rightarrow \tau^+ \tau^- \tau^+ \tau^-$  mode from HS production with leptonic decays of the  $W$  bosons can give a very clean, almost background free signal. The lepton coming from the  $W$  decay is used for the triggering of the event using the CMS single isolated lepton trigger with the thresholds 19 GeV and 26 GeV, respectively, for the muon and electron [42]. The final state  $\ell + \mu\tau_{\text{jet}}\mu\tau_{\text{jet}}$  ( $\ell = e$  or  $\mu$ , where the lepton comes from  $W$  decay) has been considered and  $\tau$  jets with one track have been selected. For each  $\tau$ -jet candidate there must be a muon in a cone 0.6 around the track. Unlike the VBF case, the muons are not required to have the same sign. The full list of selections is:

- trigger selection: isolated muon or electron with  $p_T$  greater than 19 or 26 GeV, respectively, and  $|\eta| < 2.5$ ;
- two 1-prong  $\tau$  jets with  $p_T > 10$  GeV,  $|\eta| < 2.1$ . For each  $\tau$  jet one muon of  $p_T > 7$  GeV within a cone 0.6 around the  $\tau$  track should exist and have a charge opposite to the track charge;
- events with extra jets in addition to the two  $\tau$  jets are rejected.

The results in Fig. 6 show that, after our final scan, the population of parameter points is such that in both channels the highest cross sections are found for  $M_{h_1} \gtrsim M_Z$ , although in the case of VBF also lower  $h_1$  masses can yield sizable rates. Independently of  $M_{h_1}$ , the  $a_1$  mass enables sizable event rates anywhere above  $2m_\tau$ , but particularly just above the threshold. At high luminosity,  $100 \text{ fb}^{-1}$ , the highest rates would correspond to 1000 events per year for HS and 8000 for VBF. The black diamond symbols in Fig. 6 denote the two NMSSM benchmark points P2 (right point) and P3 (left point), defined in [18, 20].

As it can be appreciated, they correspond to event rates that are mid range amongst all those explored, hence not particularly biased towards a far too favourable NMSSM setup, yet susceptible to experimental discovery.

## 4 Conclusions

We have analysed the CP-even Higgs boson  $h_1$  in the NMSSM decaying into  $a_1 a_1$  pairs in turn yielding four  $\tau$  leptons, produced at the LHC in HS and VBF production and searched for through their semi-leptonic/hadronic decays into muons and jets. We have found that there is significant potential, especially via the VBF production channel, to discover a Higgs boson at the LHC in NMSSM scenarios with  $M_{a_1} < 2m_b$  which is an important step in establishing a no-lose theorem for the NMSSM. In order to achieve this the same sign di-muon trigger with lower threshold [43] is crucial. We have restricted ourselves to the case  $M_{a_1} < 2m_b$ , where the  $h_1$  decay fraction into  $\tau$ 's is enhanced (otherwise  $a_1 \rightarrow b\bar{b}$  decays are dominant). A scan of the low-energy NMSSM parameter space without assuming unification at the high scale has shown that the  $h_1$  state can be very light, indeed at times lighter than the  $a_1$ . This configuration does not take place in the constrained NMSSM (cNMSSM) of Ref. [18, 19]. However, we are currently investigating whether such light  $h_1$  masses can be found in the NMSSM with non-universal boundary conditions at the unification scale [44]. With reference to the NMSSM benchmark points defined in [18, 20], we note that those relevant to our  $4\tau$  channel are the P2 and P3 benchmarks, which yield event rates in the mid range amongst those explored here. Our summary is preliminary, as only signal processes have been considered and only in presence of MC simulations, with no backgrounds and full detector performance enabled. The latter clearly ought to be investigated before drawing any firm conclusions and this is currently being done. However, we would like to conclude that the  $2\mu + 2$ jets signature from  $h_1 \rightarrow a_1 a_1 \rightarrow 4\tau$  decays with the  $h_1$  produced in HS and VBF processes does produce sizable event rates as high as 1000 events per year for HS and 8000 for VBF so that we expect that a significant part of the viable NMSSM parameter space will be covered by using the signature and selection cuts suggested in our study.

## References

- [1] H. P. Nilles, M. Srednicki and D. Wyler, Phys. Lett. B **120** (1983) 346.
- [2] J. M. Frere, D. R. T. Jones and S. Raby, Nucl. Phys. B **222** (1983) 11.
- [3] J. R. Ellis, J. F. Gunion, H. E. Haber, L. Roszkowski and F. Zwirner, Phys. Rev. D **39** (1989) 844.
- [4] M. Drees, Int. J. Mod. Phys. A **4** (1989) 3635.
- [5] U. Ellwanger, Phys. Lett. B **303** (1993) 271.
- [6] U. Ellwanger, M. Rausch de Traubenberg and C. A. Savoy, Phys. Lett. B **315** (1993) 331.

- [7] T. Elliott, S. F. King and P. L. White, *Phys. Rev. D* **49** (1994) 2435.
- [8] P. N. Pandita, *Z. Phys. C* **59** (1993) 575.
- [9] U. Ellwanger, M. Rausch de Traubenberg and C. A. Savoy, *Z. Phys. C* **67** (1995) 665.
- [10] S. F. King and P. L. White, *Phys. Rev. D* **52** (1995) 4183.
- [11] F. Franke and H. Fraas, *Int. J. Mod. Phys. A* **12** (1997) 479.
- [12] U. Ellwanger, M. Rausch de Traubenberg and C. A. Savoy, *Nucl. Phys. B* **492** (1997) 21.
- [13] D. J. Miller, R. Nevzorov and P. M. Zerwas, *Nucl. Phys. B* **681** (2004) 3.
- [14] C. Panagiotakopoulos and K. Tamvakis, *Phys. Lett. B* **469** (1999) 145.
- [15] C. Panagiotakopoulos and A. Pilaftsis, *Phys. Rev. D* **63** (2001) 055003.
- [16] A. Dedes, C. Hugonie, S. Moretti and K. Tamvakis, *Phys. Rev. D* **63** (2001) 055009.
- [17] C. Hugonie and S. Moretti, *In the Proceedings of APS / DPF / DPB Summer Study on the Future of Particle Physics (Snowmass 2001), Snowmass, Colorado, 30 Jun – 21 Jul 2001, pp P108* [arXiv:hep-ph/0110241].
- [18] A. Djouadi *et al.*, arXiv:0801.4321 [hep-ph].
- [19] A. Djouadi, U. Ellwanger and A. M. Teixeira, arXiv:0803.0253 [hep-ph].
- [20] A. Djouadi, U. Ellwanger, R. Godbole, C. Hugonie, S.F. King, S. Lehti, S. Moretti, A. Nikitenko, I. Rottländer, M. Schumacher and A. M. Teixeira, in arXiv:0803.1154 [hep-ph].
- [21] J. F. Gunion, H. E. Haber and T. Moroi, *In the Proceedings of 1996 DPF / DPB Summer Study on New Directions for High-Energy Physics (Snowmass 96), Snowmass, Colorado, 25 Jun – 12 Jul 1996, pp LTH095* [arXiv:hep-ph/9610337].
- [22] U. Ellwanger, J. F. Gunion and C. Hugonie, arXiv:hep-ph/0111179.
- [23] G. Azuelos *et al.*, arXiv:hep-ph/0204031.
- [24] U. Ellwanger, J. F. Gunion, C. Hugonie and S. Moretti, arXiv:hep-ph/0305109.
- [25] U. Ellwanger, J. F. Gunion, C. Hugonie and S. Moretti, arXiv:hep-ph/0401228.
- [26] D. J. Miller and S. Moretti, arXiv:hep-ph/0403137.
- [27] K. A. Assamagan *et al.*, arXiv:hep-ph/0406152.
- [28] G. Weiglein *et al.*, *Phys. Rept.* **426** (2006) 47.

- [29] S. Moretti, S. Munir and P. Poulose, Phys. Lett. B **644** (2007) 241.
- [30] E. Accomando *et al.*, arXiv:hep-ph/0608079.
- [31] M. Carena, T. Han, G. Y. Huang and C. E. M. Wagner, arXiv:0712.2466 [hep-ph].
- [32] S. Baffioni, talk presented at “GdR Supersymétrie 2004”, 5-7 July 2004, Clermont-Ferrand, France.
- [33] T. Sjostrand, S. Mrenna and P. Skands, JHEP **0605** (2006) 026.
- [34] U. Ellwanger, J. F. Gunion and C. Hugonie, JHEP **0502** (2005) 066.
- [35] U. Ellwanger and C. Hugonie, Comput. Phys. Commun. **175** (2006) 290.
- [36] F. Domingo and U. Ellwanger, arXiv:0710.3714 [hep-ph].
- [37] D. N. Spergel *et al.* (WMAP Collaboration), arXiv:astro-ph/0603449.
- [38] R. Barate *et al.* (LEP Higgs Working Group), Phys. Lett. B **565** (2003) 61.
- [39] The ALEPH, DELPHI, L3, OPAL collaborations and LEP Higgs Working Group, arXiv:hep-ex/0602042.
- [40] D. J. Miller, S. Moretti and R. Nevzorov, arXiv:hep-ph/0501139.
- [41] CMS Physics TDR, Volume II, CERN/LHCC 2006-021, CMS TDR 8.2, 26 June 2006.
- [42] The CMS Trigger and Data Acquisition project, Volume II, CERN/LHCC 2002-26, CMS TDR 6.2, 15 Dec. 2002.
- [43] The CMS High Level Trigger, CERN/LHCC 2007-021, LHCC-G-134, 29 June 2007.
- [44] A. Belyaev, S. Hesselbach and S. Moretti, *work in progress*.